Matrix Effects on Interdiffusion at the Polystyrene and Poly(vinyl methyl ether) Interface

Esmaiel Jabbari and Nikolaos A. Peppas*

School of Chemical Engineering, Purdue University, West Lafayette, Indiana 47907-1283

Received June 16, 1994; Revised Manuscript Received May 3, 1995®

ABSTRACT: The effect of polystyrene (PS) matrix relaxation on interdiffusion at a PS and poly(vinyl methyl ether) (PVME) interface was investigated with attenuated total internal reflectance infrared spectroscopy (ATR-FTIR) at 105 and 85 °C, corresponding to 5 °C above and 15 °C below the T_g of PS, respectively. Monodisperse PS samples with $\bar{M}_w$ of 3.0×10^6 and 1.05×10^5 were used to simulate relaxation in the PS matrix corresponding to chain reptation and constrained-release mechanisms, respectively. A binary blend of monodisperse PS samples consisting of short chains with $\bar{M}_w$ of 3.0×10^4 and long chains with $\bar{M}_w$ of 3.0×10^6 was used to simulate relaxation in the PS matrix by tube dilation. In the binary PS blend, the short chains were deuterated in order to monitor the concentration of each component independently. Non-Fickian diffusion was observed above and below the T_g of the PS matrix. Above the T_g of PS, interdiffusion was enhanced as the matrix relaxation mechanism changed from chain reptation to tube dilation to constrained release, consistent with the predicted relaxation time of these matrices. Below the T_g of PS, interdiffusion was controlled by the rate of swelling of PS by PVME and interdiffusion was faster in the binary PS blend due to the reduced entanglement density between the long chains.

Introduction

Diffusion at polymer–polymer interfaces affects the polymer concentration profile and their interfacial thickness.[1–4] Polymer–polymer interdiffusion has been studied by a variety of techniques[5] including neutron and ion scattering,[6–8] X-ray fluorescence,[9] electron microscopy,[10–12] Raman and infrared spectroscopy,[13–19] and light scattering.[20,21] These studies have provided evidence for the importance of temperature,[22] molecular weight,[23] molecular weight distribution,[24] and composition[25,26] on interdiffusion at polymer–polymer interfaces. More importantly, these studies have shown that interdiffusion at polymer–polymer interfaces is controlled by the slower or faster diffusing component below and above the glass transition, T_g, of the slow-diffusing component, respectively.[27–30]

In our previous paper,[15] we observed non-Fickian diffusion at the polystyrene (PS) and poly(vinyl methyl ether) (PVME) interface both below and above the T_g of the slow-diffusing component, PS, in which interdiffusion was partially controlled by the relaxation of the slow-diffusing component. This non-Fickian behavior at the PS/PVME interface has also been observed by Sauer and Walsh[20] and Deppe et al.[31] We used a combination of Fickian and case II models to fit the experimental results. The data at 105 and 85 °C, corresponding to 5 and 15 °C above and below the T_g of PS, had 20% and 70% non-Fickian component, respectively. In another paper,[32] the swelling of PS by PVME was confirmed with dynamic mechanical analysis using cross-linked PS in contact with PVME. We showed that the swelling process was characterized by an interfacial velocity as the PVME swelled the PS matrix. The relaxation time of the swelling process was determined from the interface velocity as a function of temperature, and the results indicated that the swelling process was controlled by the relaxation time of the slowly diffusing component, PS.

We also investigated[24] the effect of molecular weight and polydispersity on interdiffusion at the PS/PVME interface. According to these results, interdiffusion was independent of PS molecular weight but strongly dependent on PVME molecular weight in good agreement with the fast mode theory[28,29] in which interdiffusion is controlled by the faster diffusing component, PVME. Furthermore, the molecular weight distribution of PS significantly affected the rate of interdiffusion across the interface. It was shown that tube renewal significantly affected the relaxation of the PS matrix as low molecular weight PS with molecular weight below the entanglement was added to the matrix. This indicated that interdiffusion can be significantly affected by the mechanism of the matrix relaxation.

The effect of the mechanism of matrix relaxation on the viscoelastic properties of polydisperse polymer systems[33–36] and binary or ternary blends of monodisperse polymers[37–41] has been studied recently. These results indicate that different matrix relaxation mechanisms such as chain reptation,[42–45] tube dilation,[46] tube renewal,[47] or constrained release[48,49] can significantly affect the terminal relaxation time and the zero-shear viscosity of polymer melts. We believe that the relaxation-controlled interdiffusion at the PS/PVME interface was undoubtedly related to the mechanism of relaxation of the PS matrix.

Here, we report on the effect of matrix relaxation on interdiffusion at the PS/PVME interface above and below the T_g of the slow-diffusing component, PS. The technique of attenuated total internal reflectance infrared spectroscopy (ATR-FTIR) is used for measuring interdiffusion. With ATR-FTIR, the diffusion of each component can be monitored independently without labeling because polymers have specific absorption bands in the infrared region, and the concentration of each component in a matrix consisting of a binary blend of polymers can be measured by deuteration.

Three PS matrices with different relaxation mechanisms were constructed using PS samples of different molecular weight or a binary blend of monodisperse PS samples. Monodisperse PS samples with $\bar{M}_w$ of 3.0×10^6 and 1.05×10^5 were used to represent matrix

* Corresponding author.

® Abstract published in *Advance ACS Abstracts,* August 1, 1995.

0024-9297/95/2228-6229$09.00/0

relaxation by chain reptation and constrained release, respectively. A binary blend of two monodisperse PS samples with 75 wt % PS of $\bar{M}_w$ 3.0 × 10^6 and 25 wt % PS of $\bar{M}_w$ 3.0 × 10^4 was constructed to represent matrix relaxation by tube dilation.

Experimental Section

Polystyrene samples with weight-average molecular weights, $\bar{M}_w$, of 3.0 × 10^4, 1.05 × 10^5, and 3.0 × 10^6 and polydispersity indices of lower than 1.06 were obtained from Pressure Chemical Co. (Pittsburgh, PA) as primary standards. PVME was obtained from Scientific Polymer Products (Ontario, NY) as a secondary standard with $\bar{M}_w$ of 9.9 × 10^4 and a polydispersity index of 2.10. Gel permeation chromatography analysis of the two polymers indicated that no additives were present. The GPC was carried out with a GPC system (Model 6000A, Waters Associates, Milford, MA) with tetrahydrofuran as the solvent and μ-Styragel columns with 10^6-, 10^5-, and 10^3-Å pore sizes and a 1 mL/min flow rate. The PS and PVME samples had T_g of +101 and −27 °C, respectively, measured by differential scanning calorimetry (DSC 2910, E. I. du Pont de Nemours & Co., Wilmington, DE).

Monodisperse PS with $\bar{M}_w$ of 3.0 × 10^4 was ring deuterated for studying interdiffusion in binary blends of monodisperse PS samples. The benzene ring hydrogens of PS were deuterated using excess deuterated benzene in the presence of catalytic amounts of ethylaluminum chloride ($EtAlCl_2$) and anhydrous hydrogen chloride at room temperature and under nitrogen.[50-52] Deuterated benzene and ethylaluminum dichloride ($EtAlCl_2$) were purchased from Aldrich Chemical Co. (Milwaukee, WI) and used without further purification. Anhydrous gaseous hydrogen chloride was prepared from the reaction of sodium chloride and concentrated sulfuric acid and passed through concentrated sulfuric acid and mercury traps. In a typical procedure, a 50-mL reaction flask was charged with 1 g of monodisperse PS with $\bar{M}_w$ of 3.0 × 10^4 and 20 mL of deuterated benzene under nitrogen. Next, catalytic amounts of $EtAlCl_2$ were added to the mixture followed by the addition of gaseous HCl at room temperature and under nitrogen. The reaction mixture was stirred vigorously for 4 h, quenched with 3 mL of distilled water, washed three times with distilled water, and dried over anhydrous sodium sulfate. After drying, the deuterated PS was isolated by precipitation in *n*-hexane and filtered. The white solid product was dried in vacuo for 24 h at room temperature.

The deuterated PS was characterized by ^1H NMR, FTIR, GPC, and DSC. ^1H NMR was recorded in $CDCl_3$ using a Varian XL-200 NMR instrument. The extent of deuteration was calculated by comparing the integration ratio of the aliphatic methyl protons and aromatic protons of normal PS with deuterated PS. The complete disappearance of the peaks due to aromatic protons at around 6.5 and 7.1 ppm was used for monitoring the extent of deuteration. The extent of deuteration was more than 99%.

A FTIR spectrometer (Nicolet 800, Madison, WI) with the ATR accessory (Connecticut Instruments) was used for the interdiffusion studies.[15] The ATR crystal was germanium with 5-cm length, 1-cm width, and 2-mm thickness. The PS film was cast on the ATR crystal with a spin coater (Model 11-EC10D-R485, Photo-Resist Spinners, Garland, TX) from a *p*-xylene solution. PS with $\bar{M}_w$ of 3.0 × 10^6 was used to simulate a PS matrix with only reptation as the mechanism of chain relaxation, henceforth designated by the PS3M matrix. The PS3M film was spin cast on the ATR crystal from a 2 wt % *p*-xylene solution at 400 rpm. PS with $\bar{M}_w$ of 1.05 × 10^5 was used to simulate a PS matrix with constraint release or tube reorganization[49] as the mechanism of chain relaxation, henceforth designated by the PS100K matrix. The PS100K film was spin cast on the ATR crystal from a 5 wt % *p*-xylene solution at 250 rpm. A binary blend consisting of 75 and 25 wt % monodisperse PS samples with $\bar{M}_w$ of 3.0 × 10^6 and 3.0 × 10^4, respectively, was used to simulate a PS matrix with tube dilation[46] as the mechanism of chain relaxation, henceforth designated by PShd. The PShd film was spin cast on the ATR crystal from a 2 wt % *p*-xylene solution at 400 rpm.

The PS films were dried in a controlled atmosphere at 25 °C for at least 24 h, then dried in vacuo at 25 °C for 24 h, and finally heated to 115 °C to remove any residual solvent and minimize molecular orientation resulting from the spinning process. The thicknesses of the PS films were measured using a profilometer (alpha-step 200, Tencor Instruments, Mountain View, CA). The PVME was cast directly on the PS film from a 10 wt % isobutyl alcohol solution at 250 rpm. The PVME film was dried at 25 °C for 24 h and then dried in vacuo at room temperature for 24 h to remove residual solvent. Since the T_g of PVME is below room temperature, further drying at higher temperatures was not necessary. The thickness of the PVME film was measured using the procedure described in ref 15.

The use of ATR-FTIR for interdiffusion studies at polymer−polymer interfaces was described by us before.[15,24,26,32] Briefly, the infrared beam enters the ATR crystal from one of the side faces. If the refractive index of the crystal is higher than that of PS and the incident angle of the beam is higher than a critical angle, then the infrared beam is totally reflected at the crystal/PS interface and, the beam travels inside the crystal and exits from the other side face. At the crystal/polymer interface, a small fraction of the beam penetrates into the PS layer and is absorbed by PS.[53] The fraction of the beam which is absorbed gives rise to absorption bands in the ATR spectrum which can be used to monitor the concentration of each component within the penetration depth of the polymer layer.

In a typical ATR-FTIR experiment, a PS film was cast by spin coating from a *p*-xylene solution on a Ge crystal. The PS film was dried in a controlled atmosphere to remove any residual solvent. The PVME was spin cast directly on the PS film from an isobutyl alcohol solution to ensure good molecular contact at the PS/PVME interface. The assembly consisting of the ATR crystal, the two polymer films, the aluminum foil, and the heating unit was heated to the desired interdiffusion temperature, and the ATR-FTIR spectrum was collected in situ with 128 averaged scans and a resolution of 4 cm^{-1}. The end-face angle of the ATR crystal and the optical angle of the infrared beam were 45°.

Spectral Analysis

The benzene ring hydrogens of a monodisperse PS with $\bar{M}_w$ of 3.0 × 10^4 were deuterated in the presence of deuterated benzene and HCl and catalytic amounts of $EtAlCl_2$ at room temperature and under a nitrogen atmosphere. Parts a and b of Figure 1show the ^1H NMR spectra of PS before and after the deuteration reaction, respectively. The peaks centered at 1.45 and 1.85 ppm are due to the hydrogens of the aliphatic main chain of PS. The peaks centered at 6.60 and 7.05 ppm are due to hydrogens of the aromatic ring. The loss of aromatic hydrogen peaks, as evidenced in the spectrum of deuterated PS, is an indication of deuteration. The extent of deuteration was determined by comparing the ratio of the aliphatic and aromatic methyl protons of normal PS with that of deuterated PS. According to ^1H NMR results, the extent of deuteration was greater than 99%.

The molecular weight distribution of the PS before and after deuteration was measured with GPC, as shown in parts a and b of Figure 2. Figure 2a is the GPC trace of PS with $\bar{M}_w$ of 3.0 × 10^4 and polydispersity index of 1.06 before the deuteration reaction. Figure 2b compares the GPC trace of monodisperse PS after the deuteration reaction (curve 1) with a commercially available polydisperse aromatic deuterated PS with $\bar{M}_w$ of 1.0 × 10^5 and polydispersity index of 2.5 (curve 2). Comparison of the GPC traces in Figure 2b indicates that the deuteration reaction did not alter the molecular weight or the molecular weight distribution of the PS.

The FTIR spectra of PS before and after the deuteration reaction, in the 3500−2000 cm^{-1} range, are shown

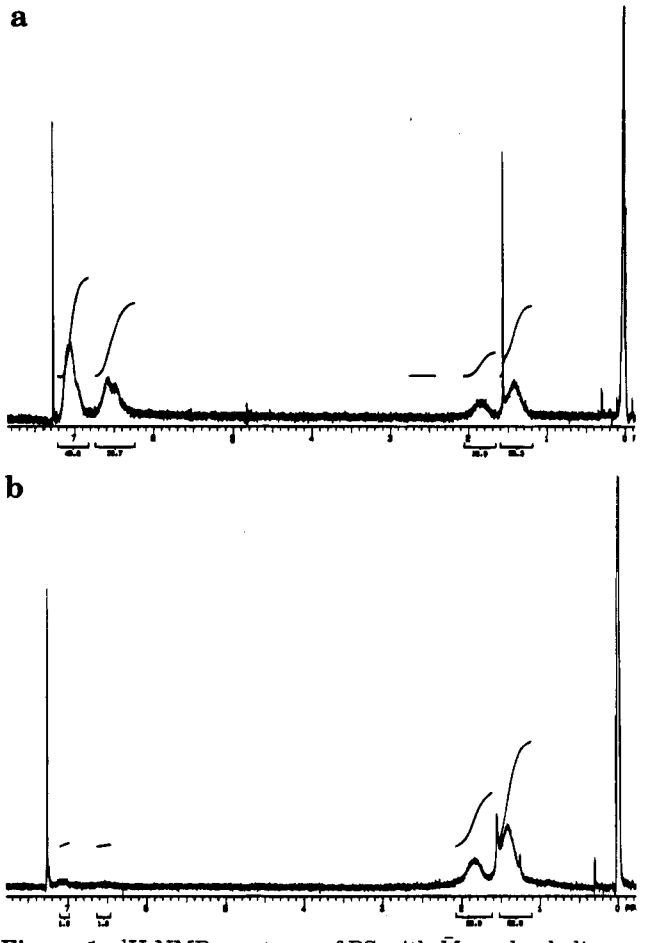

Figure 1. ^{1}H-NMR spectrum of PS with $\bar{M}_w$ and polydispersity index of 3.0 × 10^4 and 1.06, respectively, before the deuteration reaction. The peaks centered at 1.45 and 1.85 ppm are due to the aliphatic hydrogens of PS. The peaks centered at 6.60 and 7.05 ppm are due to the aromatic hydrogens of PS. (b) ^{1}H-NMR spectrum of PS with $\bar{M}_w$ and polydispersity index of 3.0 × 10^4 and 1.06, respectively, after the deuteration reaction. The peaks centered at 1.45 and 1.85 ppm are due to the aliphatic hydrogens of PS. The peaks at 6.60 and 7.05 ppm have disappeared after the deuteration reaction.

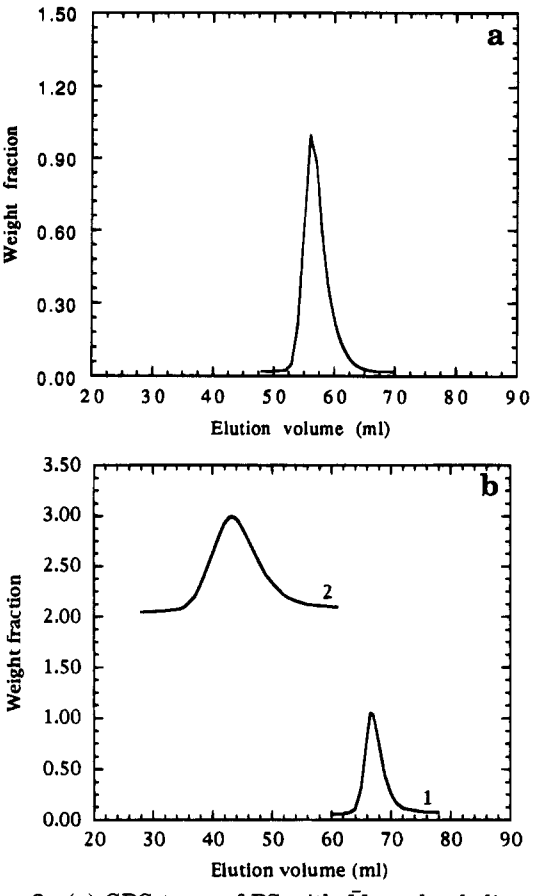

Figure 2. (a) GPC trace of PS with $\bar{M}_w$ and polydispersity index of 3.0 × 10^4 and 1.06, respectively, before the deuteration reaction. (b) GPC traces for PS with $\bar{M}_w$ and polydispersity index of 3.0 × 10^4 and 1.06, respectively, after the deuteration reaction (curve 1) and a commercially available polydisperse deuterated PS with $\bar{M}_w$ and polydispersity index of 1.0 × 10^5 and 2.5, respectively (curve 2). The weight fraction scale corresponds to curve 1. Curve 2 is shifted by 2.0 units for visual clarity.

in parts a and b of Figure 3, respectively. The high-frequency spectra of PS consists of seven absorption bands (Figure 3a).[52] The bands with peak locations at 2930 and 2850 cm^{-1} are due to the C-H stretching vibrations of the CH_2 and CH groups of the aliphatic main chain. The bands with peak locations at 3000, 3030, 3060, 3085, and 3105 cm^{-1} are due to the C-H stretching of the aromatic CH groups on the PS side chain. The five bands due to aromatic CH groups move to a lower frequency centered at 2250 cm^{-1} for deuterated PS, as shown in Figure 3b. Figure 3b compares the spectra of PS after the deuteration reaction (curve 1) with that of a commercially available polydisperse deuterated PS indicating that the deuteration reaction was complete.

The ATR-FTIR spectra of PS and PVME in the high-frequency region and the assignment of each absorption band were previously discussed by us.[15] The ATR-FTIR spectrum of a 50/50 (w/w) PS/PVME in the high-frequency region from 2700 to 3200 cm^{-1} is shown in Figure 4. Band 1 with peak position at 2820 cm^{-1} is the C−H stretching of the CH_3 group of the PVME methoxy side chain. Bands 3−5 with peak positions at 2880, 2930, and 2975 cm^{-1} are due to the C−H stretching vibration of the CH_2 and CH groups on the PVME main chain. Bands 2 and 4 with peak positions at 2850 and 2930 cm^{-1} are due to the C−H stretching vibration of the CH and CH_2 groups on the PS main chain, respectively. Bands 6−10 are due to the C−H stretching of aromatic CH groups on the PS side chain, as discussed previously, and these bands are absent in the spectra of deuterated PS. The seven absorption bands of PS and the four absorption bands of PVME in the high-frequency region combine to give 10 bands with the PS and PVME bands at 2930 cm^{-1} superimposed.

The PVME band at 2820 cm^{-1} and the PS bands at 2850 and 3030 cm^{-1} were used to determine the mole fraction of PVME as a function of interdiffusion time. To relate the molar fraction of PVME to the relative absorbance of PVME and PS, a calibration curve was constructed. Blends of PS and PVME with known compositions ranging from 10 to 90% by weight were cast from a toluene solution on ATR crystals, and their spectra were collected. The areas under the peaks were determined by deconvoluting[15] the spectrum. The areas of the PVME band at 2820 cm^{-1} and the PS bands at 2850 and 3030 cm^{-1} were used to calculate the relative absorption of PVME and PS. Figure 5 shows a typical time evolution of ATR-FTIR spectra for the PS/PVME pair at 105 °C with PS and PVME $\bar{M}_w$ of 1.05 × 10^5 and 9.9 × 10^4 and polydispersity indices of 1.06 and 2.10, respectively. The PS and PVME film thicknesses were 0.7 and 6.6 μm, respectively. The spectra 1−10 correspond to 0, 21, 42, 63, 84, 105, 139, 199, 259, and

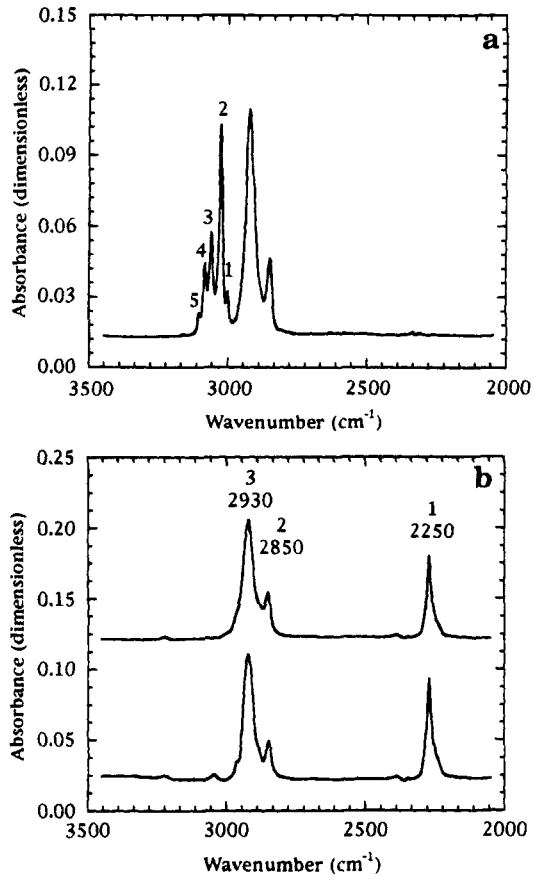

Figure 3. (a) FTIR spectra of PS with $\bar{M}_w$ and polydispersity index of 3.0×10^4 and 1.06, respectively, before the deuteration reaction in the high-frequency region. The absorption bands 1–5 with peak locations at 3000, 3030, 3060, 3085, and 3105 cm^{-1} are due to the C–H stretching vibrations of the aromatic CH groups on the PS side chain. (b) FTIR spectra of PS with $\bar{M}_w$ and polydispersity index of 3.0×10^4 and 1.06, respectively, after the deuteration reaction (curve 1) and a commercially available polydisperse deuterated PS with $\bar{M}_w$ and polydispersity index of 1.0×10^5 and 2.5, respectively (curve 2). The absorption band 1 with peak location at 2250 cm^{-1} is due to the C–D stretching vibration of the aromatic CD groups on the deuterated PS side chain. The absorption bands 2 and 3 with peak locations at 2850 and 2930 cm^{-1} are due to the C–H stretching vibrations of the aliphatic CH and CH_2 groups on the PS main chain, respectively. The absorbance scales for curves 1 and 2 were shifted by 0.025 and 0.125 units, respectively, for visual clarity.

319 min of interdiffusion, respectively. The absorbance scale corresponds to the spectrum at zero interdiffusion time. The other spectra were shifted by 0.01 absorbance unit for visual clarity. According to Figure 5, as interdiffusion proceeds, the PVME band at 2820 cm^{-1} increases with time, while the PS bands at 2850 and 3030 cm^{-1} decrease with time. The spectra were deconvoluted, the relative absorption of PVME as a function of time was calculated, and the molar fraction of PVME was obtained from the calibration curve.

Figure 6 shows the effect of PS matrix relaxation on interdiffusion at a PS/PVME interface at 105 °C, corresponding to 5 °C above the T_g of the PS matrix. Figure 7 shows the same effect on interdiffusion in a PS/PVME pair at 85 °C, corresponding to 15 °C below the T_g of the PS matrix. In Figures 6 and 7, the open and filled circles correspond to a constrained-release matrix (PS100K) with PS $\bar{M}_w$ of 1.05×10^5 and a reptation matrix with PS $\bar{M}_w$ of 3.0×10^6 (PS3M), respectively, and the open squares correspond to a tube dilation matrix (PShd) consisting of a binary blend of

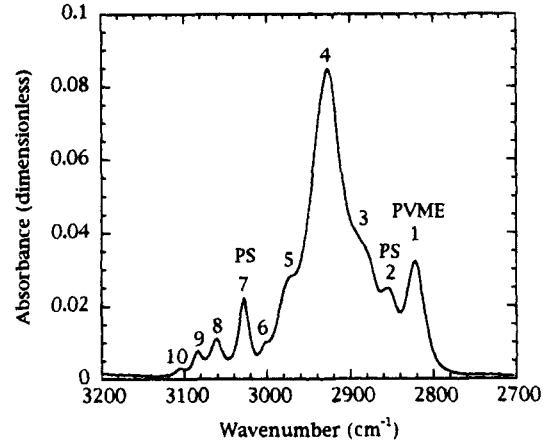

Figure 4. ATR-FTIR spectrum of a 50/50 (w/w) PS/PVME mixture in the high frequency region. Absorption bands 1–10 correspond to peak frequencies of 2820, 2850, 2880, 2930, 2975, 3000, 3030, 3060, 3085, and 3105 cm^{-1}, respectively.

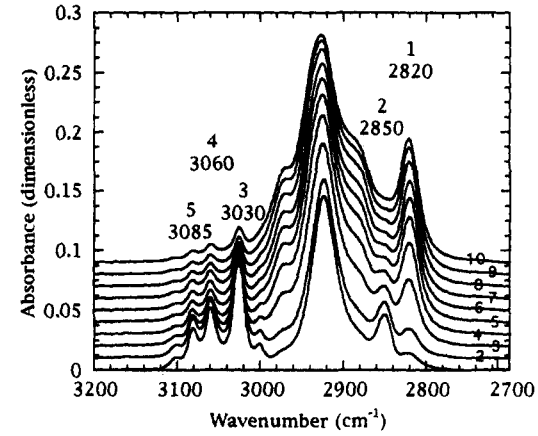

Figure 5. Time evolution of the ATR-FTIR spectra for interdiffusion at a PS/PVME interface at 105 °C. The PS and PVME $\bar{M}_w$s were 1.05×10^5 and 9.9×10^4 and polydispersity indices were 1.06 and 2.10, respectively. The PS and PVME film thicknesses were 0.7 and 6.6 μm, respectively. The spectra 1–10 correspond to 0, 21, 42, 63, 84, 105, 139, 199, 259, and 319 min of interdiffusion time, respectively. The absorbance scale corresponds to the spectrum at zero interdiffusion time, and the other spectra were shifted by 0.01 unit for visual clarity.

monodisperse PS and deuterated PS with 75 and 25 weight fractions and $\bar{M}_w$ of 3.0×10^6 and 3.0×10^4, respectively. The PS film thicknesses for experiments with PS100K, PS3M, and PShd matrices were 0.7, 0.45, and 0.40 μm, respectively. The dimensionless Fourier time in Figures 6 and 7 is defined by:

$$t^* = tD_{PV}/\delta_1^2 \quad (1)$$

Here, t^* and t are dimensionless and experimental times, respectively, D_{PV} is the self-diffusion coefficient of PVME, and δ_1 is the thickness of the PS layer.

For the experiments with binary blends of monodisperse PS, the mole fraction of high molecular weight PS with $\bar{M}_w$ of 3.0×10^6 was determined using the bands with peak locations at 3030, 3060, and 3085 cm^{-1} due to the C–H stretching of aromatic CH groups on the PS side chain. The bands were deconvoluted to determine the area under the peaks, and they were normalized based on the area of the reference band with peak location at 2930 cm^{-1} which is the common peak for PS, deuterated PS, and PVME. Figure 8 shows the time evolution of the ATR-FTIR spectra for a binary

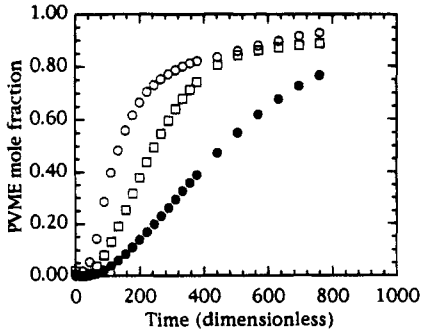

Figure 6. Effect of the mechanism of PS matrix relaxation on the PVME cumulative concentration at a PS/PVME interface at 105 °C. The open and filled circles correspond to matrices with constrained release (PS100K) and chain reptation (PS3M) as the mechanism of matrix relaxation, respectively. The open squares correspond to a tube dilation matrix (PShd) consisting of a binary blend of monodisperse normal PS and deuterated PS with weight fractions of 75 and 25 and $\bar{M}_w$s of 3.0×10^6 and 3.0×10^4, respectively. The PS film thicknesses for PS100K, PS3M, and PShd matrices were 0.7, 0.45, and 0.40 μm, respectively. The PVME $\bar{M}_w$ and polydispersity index were 9.9×10^4 and 2.10, respectively, with a film thickness of 6.6 μm.

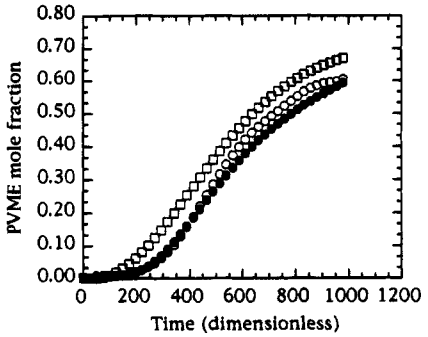

Figure 7. Effect of the mechanism of PS matrix relaxation on the PVME cumulative concentration at a PS/PVME interface at 85 °C. The open and filled circles correspond to matrices with constrained release (PS100K) and chain reptation (PS3M) as the mechanism of matrix relaxation, respectively. The open squares correspond to a tube dilation matrix (PShd) consisting of a binary blend of monodisperse normal PS and deuterated PS with weight fractions of 75 and 25 and $\bar{M}_w$s of 3.0×10^6 and 3.0×10^4, respectively. The PS film thicknesses for PS100K, PS3M, and PShd matrices were 0.7, 0.45, and 0.40 μm, respectively. The PVME $\bar{M}_w$ and polydispersity index were 9.9×10^4 and 2.10, respectively, with a film thickness of 6.6 μm.

blend of monodisperse PS and deuterated PS in contact with PVME at 85 °C. The binary PS blend in Figure 8 consisted of 75 and 25 wt % monodisperse PS and deuterated PS with $\bar{M}_w$ of 3.0×10^6 and 3.0×10^4, respectively. The molecular weight and polydispersity index of PVME was 9.9×10^4 and 2.10, respectively. The PS and PVME film thicknesses were 0.4 and 6.6 μm, respectively. The spectra 1–8 correspond to 0, 1.3, 3.0, 4.7, 6.0, 7.7, 9.0, and 10.7 h of interdiffusion time, respectively. The absorbance scale corresponds to the spectrum at zero interdiffusion time. The other spectra were shifted by 0.01 absorbance unit for visual clarity. According to Figure 8, as interdiffusion proceeds, the PVME band at 2820 cm^{-1} increases with time, while the PS bands at 3030, 3060, and 3085 cm^{-1} due to a nondeuterated PS component decrease as a function of time. Figures 9 and 10 show the effect of the mechanism of PS matrix relaxation on the concentration of a higher molecular weight PS component for interdiffusion at a PS/PVME interface at 105 and 85 °C, respectively. The mole fractions in Figures 9 and 10 are normalized based on one at the beginning of the experiment when the PS and PVME phases are completely separated to zero at the end of the experiment in which the deuterated PS, nondeuterated PS, and PVME are completely mixed. Therefore, the ordinate in Figures 9 and 10 is the normalized nondeuterated mole fraction of PS.

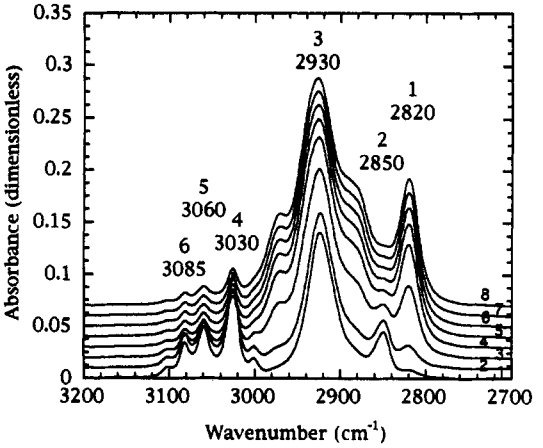

Figure 8. Time evolution of the ATR-FTIR spectra for interdiffusion at the interface between a binary blend of monodisperse normal and deuterated PS and PVME at 85 °C. The binary PS blend consisted of 75 and 25 wt % monodisperse normal and deuterated PS with $\bar{M}_w$s of 3.0×10^6 and 3.0×10^4, respectively. The PVME $\bar{M}_w$ and polydispersity index were 9.9×10^4 and 2.10, respectively. The PS and PVME film thicknesses were 0.4 and 6.6 μm, respectively. The spectra 1–8 correspond to 0, 1.3, 3.0, 4.7, 6.0, 7.7, 9.0, and 10.7 h of interdiffusion time, respectively. The absorbance scale corresponds to the spectrum at zero interdiffusion time, and the other spectra were shifted by 0.01 unit for visual clarity.

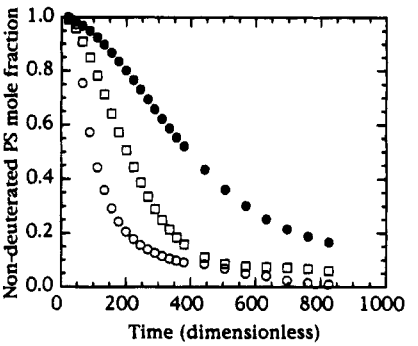

Figure 9. Effect of the mechanism of PS matrix relaxation on the cumulative concentration of the long PS chain at a PS/PVME interface at 105 °C. The open and filled circles correspond to matrices with constrained release (PS100K) and chain reptation (PS3M) as the mechanism of matrix relaxation, respectively. The open squares correspond to a tube dilation matrix (PShd) consisting of a binary blend of monodisperse normal PS and deuterated PS with weight fractions of 75 and 25 and $\bar{M}_w$ of 3.0×10^6 and 3.0×10^4, respectively. The PS film thicknesses for PS100K, PS3M, and PShd matrices were 0.7, 0.45, and 0.40 μm, respectively. The PVME $\bar{M}_w$ and polydispersity index were 9.9×10^4 and 2.10, respectively, with a film thickness of 6.6 μm.

Analysis of Results

The relative intensity of infrared radiation decreases exponentially as a function of distance away from the crystal surface and is characterized by the penetration depth of infrared radiation within the polymer film.[15,53] Figures 6, 7, 9, and 10 indicate cumulative concentrations. To compare the experimental results with model

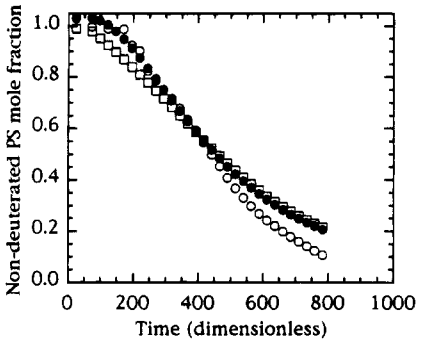

Figure 10. Effect of the mechanism of PS matrix relaxation on the cumulative concentration of the long PS chain at a PS/PVME interface at 85 °C. The open and filled circles correspond to matrices with constrained release (PS100K) and chain reptation (PS3M) as the mechanism of matrix relaxation, respectively. The open squares correspond to a tube dilation matrix (PShd) consisting of a binary blend of monodisperse normal PS and deuterated PS with weight fractions of 75 and 25 and $\bar{M}_w$ of 3.0×10^6 and 3.0×10^4, respectively. The PS film thicknesses for PS100K, PS3M, and PShd matrices were 0.7, 0.45, and 0.40 μm, respectively. The PVME $\bar{M}_w$ and polydispersity index were 9.9×10^4 and 2.10, respectively, with a film thickness of 6.6 μm.

predictions, for an interdiffusion time t, the mole fraction of PVME, C_{PV}, at distance z from the crystal surface was multiplied by its corresponding relative intensity and it was integrated over the penetration depth. This process was repeated for each interdiffusion time to give the cumulative concentration of PVME, $Q(t)$, versus time given by:[15]

$$Q(t) = \frac{\int_0^\infty C_{PV}(z,t)\, I_{rel}(z)\, \partial z}{\int_0^\infty I_{rel}(z)\, \partial z} \tag{2}$$

Here, I_{rel} is the infrared intensity relative to the intensity at the interface and z is the distance from the crystal/polymer interface in the polymer layer.

In eq 2, it is assumed that the penetration depth of IR radiation is independent of the refractive index gradient across the PS/PVME interface as interdiffusion proceeds. The effect of refractive index gradient on penetration depth was discussed previously by us.[15] In brief, the variation in refractive index across the interface was shown to be negligible for infrared frequencies, especially in the higher frequency range of 2500−3500 wavenumbers, but the variation is significant for visible light frequencies as shown by Stein and collaborators.[21] In a previous study by us,[15] error analysis was done to determine the effect of uncertainty in the values of refractive index, wavelength, and PS and PVME film thickness on the penetration depth. For 20% uncertainty in the value of refractive indices and 2% certainty in the wavelength IR radiation, there was less than 1% variation in the penetration depth. Also the effect of PVME film thickness on penetration depth was negligible. The variation in PS film thickness across the ATR crystal contributed as much as 8% error in the concentration of PVME. The effect of variation in PS film thickness on the cumulative concentration of PVME was simulated by fitting the experimental data to the Fickian model with 0.1 m variation (maximum variation expected based on surface roughness measurements with profilometer) in PS film thickness across the interface. The fit could not reproduce the shape of the PVME cumulative concentration. On the other side, a combination of Fickian and case II diffusion provided the best fit to the experimental results, especially for experiments below the T_g of PS. Therefore, the experimental results were analyzed using a combination of Fickian and case II diffusion.

For a Fickian model, the PVME concentration profile across the interface as a function of distance and time was derived by us previously and is given by:[15,24]

$$C_{PV}(z,t) = 1 - \frac{C_0}{2}\sum_{n=-\infty}^{n=+\infty}\left\{\mathrm{erf}\left[\frac{\delta_1 + 2n(\delta_1+\delta_2) - z}{2(Dt)^{1/2}}\right] + \mathrm{erf}\left[\frac{\delta_1 + 2n(\delta_1+\delta_2) + z}{2(Dt)^{1/2}}\right]\right\} \tag{3}$$

Here, C_{PV} is the molar concentration of PVME, C_0 is the initial molar concentration of PVME, D is the interdiffusion coefficient, and δ_1 and δ_2 are the PS and PVME film thicknesses, respectively. The Fickian component of the PVME cumulative concentration is obtained by substituting for C_{PV} from eq 3 in eq 2.

The case II model corresponds to a diffusion process which depends on the relaxation of the PS matrix and is independent of the concentration profile.[55] The case II diffusion is characterized by an interface velocity, K_i, which defines how fast the interface moves into the PS layer. For case II diffusion, the cumulative concentration of PVME was derived by us previously and is given by:[15,24]

$$Q_{II}(t) = C_{PV}^{eq} \exp\left[\frac{-2(\delta_1 - K_i t)}{d_P}\right] \tag{4}$$

Here, Q_{II} is the case II component of the PVME cumulative concentration, C_{PV}^{eq} is the equilibrium concentration of PVME obtained from the experimental data at long diffusion times, and d_P is the penetration depth of the infrared beam within the polymer film. The PVME cumulative concentration can be represented by a linear combination of Fickian and case II components as given by:

$$Q(t) = (1 - \phi_{II})Q_F(t) + \phi_{II}Q_{II}(t) \tag{5}$$

Here, Q is the PVME cumulative concentration, Q_F and Q_{II} are the Fickian and case II components of the cumulative concentration, respectively, and ϕ_{II} is the fraction of the case II component.

A linear combination of Fickian and case II diffusion was chosen to analyze the data because it assumes the two components of diffusion act independently and allows us to extract quantitative information such as the percent non-Fickian, the interdiffusion coefficient, and the interface velocity. The quality of the fit of the experimental data to the model was determined using the correlation coefficient, as discussed previously by us.[15] The correlation coefficient of the fit using a linear combination of Fickian and case II diffusion was better than 0.99. For the experiments at 105 °C, there was a slight improvement of the fit when a linear combination of Fickian and case II was used and the correlation coefficient improved from 0.9954 for the Fickian model to 0.99996 for the linear combination of Fickian and case II diffusion. For the experiments at 85 °C, the correlation coefficient obtained by fitting the data to the Fickian model was less than 0.85. However, the correlation coefficient increased to 0.9963 when the data

Table 1. Best Fit of the Experimental Data at 105 °C to the Fickian and Case II Models for the PS3M, PShd, and PS100K Matrices

PS matrix	% Non-Fickian component	diffusion coefficient, cm^2/s ($\times 10^{13}$)	case II interface velocity, cm/s ($\times 10^8$)
PS3M	0.30	3.0 ± 1.4	1.3 ± 0.6
PShd	0.25	4.2 ± 1.9	2.6 ± 1.2
PS100K	0.20	15.0 ± 7.0	2.7 ± 1.3

were fitted with a linear combination of Fickian and case II diffusion with 70% case II component and the shape of the experimental cumulative concentration profile was similar to the case II mode. It should be mentioned that other diffusion models or a nonlinear combination of Fickian and case II models may also give a satisfactory fit of the experimental data. To be able to distinguished between these different models, a more extensive experimental investigation with different types of PS matrices and molecular weights is required which is in progress.

Discussion of Results

The effect of the mechanism of PS matrix relaxation on interdiffusion at the PS/PVME interface at 105 °C, 5 °C above the T_g of PS, is shown in Figure 6. The open and filled circles correspond to PS100K and PS3M matrices, and the open squares correspond to the PShd matrix. For the PS3M matrix, the PS matrix is monodisperse with $\bar{M}_w$ of 3.0×10^6 which is at least 10 times greater than the critical molecular weight for the onset of reptation.[56] Therefore, for the PS3M matrix, chain reptation is the dominant mechanism of relaxation. For the PS100K matrix, The PS matrix is monodisperse with $\bar{M}_w$ of 1.05×10^5 which is less than the critical molecular weight for the onset of reptation but greater than the critical molecular weight for entanglement.[56] Therefore, for the PS100K matrix, constrained release or tube reorganization dominates the relaxation of the PS matrix.[48,49,56] For the PShd matrix, the PS matrix is a binary blend of monodisperse PS samples with $\bar{M}_w$s of 3.0×10^6 and 3.0×10^4 and 75 and 25 wt %, respectively. The concentration of the long chains is much greater than the critical concentration for the entanglement of long chains.[41] The long chains, with molecular weight much higher than the critical molecular weight for the onset of entanglement, form permanent obstacles, whereas the short chains with molecular weight close to the entanglement molecular weight form transient obstacles around the diffusing chains and cause the dilation of the tube formed by the long chains.[46] Therefore, for the PShd matrix, the relaxation of the PS matrix is enhanced by tube dilation and the molecular weight between the entanglements is increased.

According to Figure 6, interdiffusion at the PS/PVME interface increases as the mechanism of PS matrix relaxation changes from chain reptation to tube dilation to constrained release. In a previous paper,[24] we showed that interdiffusion in the PS/PVME pair is independent of the molecular weight of PS above the T_g, as predicted by the fast-mode theory.[26,28] However, according to the results in Figure 6, interdiffusion at the PS/PVME interface is influenced by the mechanism of relaxation of the PS matrix. The data in Figure 6 were analyzed using a linear combination of Fickian and case II diffusion with eq 5 in conjunction with eqs 2–4.

Table 1 gives the best fit to the data in Figure 6, with the fitted parameters being the fraction of case II component, ϕ_{II}, diffusion coefficient, D, and interface velocity, K_i. As the mechanism of PS matrix relaxation was changed from constrained release to tube dilation to tube reptation, the fraction of case II component increased from 0.20 to 0.25 to 0.30. This indicated that interdiffusion became more non-Fickian as the relaxation time of the PS matrix increased. As the matrix was changed from PS3M to PShd to PS100K, the diffusion coefficient of the Fickian model increased from 3.0 to 4.2 to 15.0 $\times 10^{-13}$ cm^2/s and the interface velocity of the case II model increased from 1.3 to 2.6 to 2.7 $\times 10^{-8}$ cm/s. The errors provided in Tables 1 and 2 for the values of the diffusion coefficient and interface velocity are the maximum experimental error due to uncertainty in the values of independent variables. These variables included the refractive index gradient, wavelength, PS and PVME film thicknesses, and area of the deconvoluted peaks.

For the PS3M matrix with $\bar{M}_w$ of 3.0×10^6, the matrix relaxation was by chain reptation and the matrix relaxation time was given by:[57]

$$\tau_{rep} = \tau_0 \frac{\bar{M}_w^3}{M_0^2 M_e} \tag{6}$$

Here, τ_{rep} is the reptation time of the chain, τ_0 is the segmental relaxation time, and $\bar{M}_w$, M_e, and M_0 are chain molecular weight, entanglement molecular weight, and segment molecular weight, respectively.

For the PShd matrix, since the weight fraction of the long chains with $\bar{M}_w$ of 3.0×10^6 is much higher than the critical concentration for entanglement of long chains, the shorter chains with $\bar{M}_w$ of 3.0×10^4 behave as diluent and cause the dilation of the tube by the long chains. Since the molecular weight of the long chains was much higher than the critical molecular weight for entanglement, the matrix relaxation was by chain reptation but the relaxation was enhanced by tube dilation given by:[58]

$$\tau_d = \tau_{rep} \phi^2 \tag{7}$$

Here, τ_d is the relaxation time of a dilated tube and ϕ is the volume fraction of the long chains.

For the PS100K matrix with $\bar{M}_w$ of 1.05×10^5, matrix relaxation is due to tube reorganization or constrained release as well as chain reptation:[46–48]

$$1/\tau_m = 1/\tau_{rep} + 1/\tau_{cr} \tag{8}$$

where

$$\tau_{cr} = 0.092 \tau_0 \frac{\bar{M}_w^5}{M_0^2 M_e^3} \tag{9}$$

Here, τ_m is the overall matrix relaxation time and τ_{rep} and τ_{cr} are the matrix relaxations due to chain reptation and constrained release, respectively.

According to eqs 6–9, as the matrix relaxation changed from chain reptation to tube dilation to tube reorganization, the matrix relaxation time decreased from 4.6×10^5 to 2.6×10^5 to 1.5×10^1 s, respectively, and the diffusion coefficient changed from 3.0×10^{-13} to 4.2×10^{-13} to 1.5×10^{-12} cm^2/s, respectively. There is good qualitative agreement between the diffusion coefficients and the predicted matrix relaxation times. However, more extensive experimental data are re-

Table 2. Best Fit of the Experimental Data at 85 °C to the Fickian and Case II Models for the PS3M, PShd, and PS100K Matrices

PS matrix	% non-Fickian component	diffusion coefficient, cm^2/s ($\times 10^{14}$)	case II interface velocity, cm/s ($\times 10^9$)
PS3M	0.60	6.5 ± 2.3	1.8 ± 1.0
PShd	0.60	3.5 ± 1.6	2.8 ± 1.3
PS100K	0.60	8.8 ± 4.1	4.4 ± 2.1

quired to obtain the exact relationship between the relaxation time of the slow-diffusing matrix and the interdiffusion coefficient.

Figure 9 shows the depletion rate of the nondeuterated PS component from the PS matrix next to the ATR crystal as a function of interdiffusion time at 105 °C. For the monodisperse PS3M and PS100K matrices, the depletion rate is the total change in PS concentration with interdiffusion time. For the PShd matrix consisting of 25% deuterated PS with $\bar{M}_w$ of 3.0×10^4 and 75% normal PS with $\bar{M}_w$ of 3.0×10^6, the depletion rate is the change in the concentration of the long-chain PS component with interdiffusion time. The depletion rate of PS follows the same trend as the change in PVME concentration, shown in Figure 6. This indicates that when the slow-diffusing matrix is a binary blend of long and short chains above the critical concentration for entanglement of long chains, interdiffusion is controlled by the long chains. This also indicates that interdiffusion in polydisperse matrices is related to the weight-average molecular weight of the matrix as opposed to a number-average molecular weight.

Figure 7 shows the effect of the mechanism of PS matrix relaxation on interdiffusion at the PS/PVME interface at 85 °C, 15 °C below the T_g of PS. The open and filled circles are the cumulative concentration of PVME for the PS100K and PS3M matrices, respectively, and the open squares are for the PShd matrix. According to Figure 7, interdiffusion is faster for the PShd matrix compared to PS100K and PS3M matrices. The experimental data in Figure 7 were analyzed with eq 5, and the best fit to the data is given in Table 2. The fraction of case II component was 0.6 for all three matrices. As the PS matrix was changed from PS100K to PS3M to PShd, the diffusion coefficient of the Fickian model did not change appreciably but the interface velocity of the case II model increased from 1.8×10^{-9} to 2.8×10^{-9} to 4.4×10^{-9} cm/s, respectively. Therefore, the higher rate of diffusion of PVME for the PShd matrix compared to PS100K and PS3M matrices can be attributed to the higher interface velocity or faster rate of swelling for the PShd matrix. The PShd matrix is a binary blend of monodisperse PS samples with short chains close to the entanglement molecular weight and long chains having much higher molecular weight for entanglement. Therefore, the short chains act as diluent and increase the effective molecular weight for entanglement in the matrix according to:[38,40]

$$M_e = M_e^\circ/\phi_{ps} \tag{10}$$

Here, M_e is the effective entanglement molecular weight, M_e° is the entanglement molecular weight for monodisperse PS, and ϕ_{ps} is the weight fraction of the long PS chains.

For a binary PS matrix with 75 wt % long chains, the molecular weight of the chains between entanglement increases from 1.8×10^4 to 2.4×10^4. This increase in molecular weight between entanglements causes an increase in the rate of swelling of the PS matrix below the T_g of PS. Sauer and Walsh[59] have also studied interdiffusion in the PS/PVME bilayer below the T_g of PS, and they have observed a significant dependence of the swelling rate on entanglement density. They found that the front velocity of PVME into PS depended strongly on the temperature and time of preannealing of the spin-coated PS layer and preannealing was especially important for higher molecular weight PS films. According to their results, the interface velocity was higher for PS films which were not annealed and lower for preannealed PS films. They attributed the higher interface velocity for nonannealed PS films to the reduced entanglement density due to spinning of PS films from solution. The entanglement density dependence of interface velocity is also a proof of the swelling process at the PS/PVME interface below the T_g of PS.

Figure 10 shows the dependence of matrix relaxation on the depletion rate of PS at 85 °C. The experimental data for the PShd matrix correspond to the depletion rate of the long chains as a function of interdiffusion time. All three matrices showed similar depletion rates, with the PShd matrix having a slightly higher depletion rate (lower PS concentration). This faster depletion rate for the PShd matrix can be attributed to a lower entanglement density as discussed above. After the PS matrix is swollen (i.e., PS mole fractions less than 0.6 in Figure 11), the depletion rate of the PS100K matrix becomes faster than those of the PS3M and PShd matrices due to the significantly shorter relaxation time of the PS100K matrix.

Conclusions

The effect of PS matrix relaxation on interdiffusion at the PS/PVME interface was studied with ATR-FTIR spectroscopy. The results were analyzed using a combination of Fickian and case II models, with the fitted parameters being the fraction of case II component, the Fickian diffusion coefficient, and the case II interface velocity. At 105 °C, 5 °C above the T_g of PS, the rate of diffusion of PVME into PS increased as the mechanism of PS matrix relaxation was changed from chain reptation to tube dilation to tube reorganization. The fraction of case II component was higher for the PS matrix with chain reptation as the mechanism of relaxation as compared to tube dilation and tube reorganization.

There was good qualitative agreement between the predicted matrix relaxation times and the experimentally determined diffusion coefficients. Deuteration was used to monitor the concentration of the long PS chains in a binary monodisperse PS matrix. The change in the concentration of the long chains with PS matrix relaxation showed the same trend as the rate of diffusion of PVME into PS. This indicated that interdiffusion, in binary PS blends above the critical molecular weight for the entanglement of long chains, is controlled by the higher molecular weight component. The effect of PS matrix relaxation on interdiffusion at PS/PVME was also studied at 85 °C, 15 °C below the T_g of PS. The interface velocity was faster for the tube dilation matrix as compared to the chain reptation and constrained release. This was attributed to the reduced entanglement density in the tube dilation matrix with a subsequent increase in the rate of swelling of PS by PVME.

Acknowledgment. This work was supported by National Institute of Health (NIH) Grant GM45027; the

ATR-FTIR spectrometer was purchased with a National Science Foundation (NSF) Grant CTS-90−07141. We thank Dr. Ankush B. Agrade for substantial technical assistance for the synthesis of deuterated polystyrene.

References and Notes

(1) Voyutskii, S. S. *J. Adhes.* **1971**, *3*, 69.
(2) Jud, K.; Kausch, H. H.; Williams, J. G. *J. Mater. Sci.* **1981**, *16*, 204.
(3) Kausch, H. H.; Tirrell, M. *Annu. Rev. Mater. Sci.* **1989**, *19*, 341.
(4) Juhue, D.; Lang, J. *Macromolecules* **1994**, *27*, 695.
(5) Tirrell, M. *Rubber Chem. Technol.* **1984**, *57*, 523.
(6) Roland, C. M.; Bohm, G. G. A. *Macromolecules* **1985**, *18*, 1310.
(7) Green, P. F.; Palmstrom, C. J.; Mayer, J. W.; Kramer, E. J. *Macromolecules* **1985**, *18*, 501.
(8) Whitlow, S. J.; Wool, R. P. *Macromolecules* **1991**, *24*, 5926.
(9) Karim, A.; Felcher, G. P.; Russell, T. P. *Polym. Prepr. (Am. Chem. Soc., Div. Polym. Chem.)* **1990**, *31* (2), 69.
(10) Price, F. P.; Gilmore, P. T.; Thomas, E. L.; Laurence, R. L. *J. Polym. Sci., Polym. Symp. Ed.* **1978**, *63*, 33.
(11) Koizumi, S.; Hasegawa, H.; Hashimoto, T. *Macromolecules* **1990**, *23*, 2955.
(12) Jabbari, E.; Peppas, N. A. *J. Appl. Polym. Sci.* **1995**, *57*, 775.
(13) Hong, P. P.; Boerio, F. G.; Clarson, S. J.; Smith, S. D. *Macromolecules* **1991**, *24*, 4770.
(14) Seggern, J. V.; Klotz, S.; Cantow, H.-J. *Macromolecules* **1989**, *22*, 3328.
(15) Jabbari, E.; Peppas, N. A. *Macromolecules* **1993**, *26*, 2175.
(16) Van Alsten, J. G.; Lustig, S. R. *Macromolecules* **1992**, *25*, 5069.
(17) Lustig, S. R.; Van Alsten, J. G.; Hsiao, B. *Macromolecules* **1993**, *26*, 3885.
(18) High, M. S.; Painter, P. C.; Coleman, M. M. *Macromolecules* **1992**, *25*, 797.
(19) Eklind, H.; Hjertberg, T. *Macromolecules* **1993**, *26*, 5844.
(20) Sauer, B. B.; Walsh, D. J. *Macromolecules* **1991**, *24*, 5948.
(21) Ye, M.; Composto, R. J.; Stein, R. S. *Macromolecules* **1990**, *23*, 4830.
(22) Gilmore, P. T.; Falabella, R.; Laurence, R. L. *Macromolecules* **1980**, *13*, 33.
(23) Jordan, E. J.; Ball, R. C.; Donald, A. M.; Fetters, L. J.; Jones, R. A. L.; Klein, J. *Macromolecules* **1988**, *21*, 235.
(24) Jabbari, E.; Peppas, N. A. *J. Mater. Sci.* **1994**, *29*, 3969.
(25) Fytas, G. *Macromolecules* **1987**, *20*, 1430.
(26) Jabbari, E.; Peppas, N. A. *Polymer* **1995**, *36*, 575.
(27) Brochard, F.; Louffroy, J.; Levinson, P. *Macromolecules* **1983**, *16*, 1638.
(28) Kramer, E. J.; Green, P. F.; Palmstrom, C. J. *Polymer* **1984**, *25*, 473.
(29) Sillescu, H. *Makromol. Chem., Rapid Commun.* **1987**, *8*, 393.
(30) Seggern, J. V.; Klotz, S.; Cantow, H.-J. *Macromolecules* **1988**, *21*, 235.
(31) Deppe, D.; Spangler, L.; Torkelson, J. *Polym. Prepr. (Am. Chem. Soc., Div. Polym. Chem.)* **1993**, *34* (2), 502.
(32) Jabbari, E.; Peppas, N. A. *J. Adhes.* **1993**, *43*, 101.
(33) Booij, H. C.; Schoffeleers, H. M.; Haex, M. M. C. *Macromolecules* **1991**, *24*, 3334.
(34) Kurata, M. *Macromolecules* **1984**, *17*, 895.
(35) Graessley, W. W.; Struglinski, M. J. *Macromolecules* **1986**, *19*, 1754.
(36) Montford, J. P.; Marin, G.; Monge, P. *Macromolecules* **1986**, *19*, 1979.
(37) Han, C. D.; Kim, J. K. *Macromolecules* **1989**, *22*, 1914.
(38) Watanabe, H.; Kotaka, T. *Macromolecules* **1987**, *20*, 535.
(39) Watanabe, H.; Kotaka, T. *Macromolecules* **1987**, *20*, 530.
(40) Watanabe, H.; Sakamoto, T.; Kotaka, T. *Macromolecules* **1985**, *18*, 1008.
(41) Watanabe, H.; Kotaka, T. *Macromolecules* **1984**, *17*, 2316.
(42) de Gennes, P.-G. *J. Chem. Phys.* **1971**, *55*, 572.
(43) de Gennes, P.-G. *J. Chem. Phys.* **1980**, *72*, 4756.
(44) Higgins, J.; McLeish, T. *Nature* **1993**, *365*, 205.
(45) Russell, T. P.; Deline, V. R.; Dozier, W. D.; Felcher, G. P.; Agrawal, G.; Wool, R. P.; Mays, J. W. *Nature* **1993**, *365*, 235.
(46) Viovy, J. L.; Rubinstein, M.; Colby, R. H. *Macromolecules* **1991**, *24*, 3587.
(47) Green, P. F. *Macromolecules* **1991**, *24*, 3373.
(48) von Seggern, J.; Klotz, S.; Cantow, H.-J. *Macromolecules* **1991**, *24*, 3300.
(49) Montfort, J.-P.; Marin, G.; Monge, P. *Macromolecules* **1984**, *17*, 1551.
(50) Lin, J.-L.; Rigby, D.; Roe, R. J. *Macromolecules* **1985**, *18*, 1609.
(51) Long, M. A.; Garnett, J. L.; Vining, R. F. W. *J. Chem. Soc., Perkin Trans. 2* **1975**, 1298.
(52) Willenberg, B. *Makromol. Chem.* **1976**, *177*, 3625.
(53) Harrick, N. J. *Internal Reflection Spectroscopy*; Wiley: New York; 1967; p 27.
(54) Lu, F. J.; Benedetti, E.; Hsu, S. L. *Macromolecules* **1983**, *16*, 1525.
(55) Berens, A. R.; Hopfenberg, H. B. *Polymer* **1978**, *19*, 489.
(56) Green, P. F.; Kramer, E. J. *Macromolecules* **1986**, *19*, 1108.
(57) Doi, M.; Edwards, S. F. *The Theory of Polymer Dynamics*; Clarendon Press: Oxford, U. K., 1986.
(58) Kavassalis, T. A.; Noolandi, J. *Macromolecules* **1989**, *22*, 2709.
(59) Sauer, B. S.; Walsh, D. J. *Macromolecules* **1994**, *27*, 432.

MA946366B